THE ASTROPHYSICAL JOURNAL, 290:627–636, 1985 March 15

MAGNETIC FIELD STRUCTURES IN ACTIVE COMPACT RADIO SOURCES

T. W. JONES,[1] L. RUDNICK,[1] H. D. ALLER,[2] M. F. ALLER,[2] P. E. HODGE,[2] AND R. L. FIEDLER[1]
Received 1984 May 18; accepted 1984 September 28

ABSTRACT

We present the analysis of simultaneous multifrequency linear polarimetry data between 1.4 GHz and 90 GHz for about 20 active, compact radio sources at six epochs from 1977 December to 1980 July. The data are reported elsewhere (Rudnick *et al.* 1985). In addition we have examined monthly 8 GHz polarization data on the same sources. The general polarization characteristics of these sources can be well described in terms of magnetic fields which are largely turbulent and slightly anisotropic. The magnetic field symmetry axes are generally aligned with the source structural axes on the milli-arcsecond scale. (OJ 287 is a notable exception.) Monte Carlo calculations indicate that observed polarization variations and in particular "rotator" polarization events can be produced in this model as a consequence of "random walks" generated through evolution of the turbulent magnetic field.

Subject headings: interferometry — interstellar: magnetic fields — polarization — radio sources: variable

I. INTRODUCTION

Compact extragalactic radio sources have yielded their secrets slowly over the years, through flux and polarization monitoring (e.g., Altschuler and Wardle 1976, Aller, Aller, and Hodge 1981), VLBI (cf., e.g., Preuss 1982), and broad-band spectral measurements (e.g., Owen, Spangler, and Cotton 1980; Jones *et al.* 1981). To complement these pictures of compact sources, we initiated a program of measuring the integrated linear polarization properties of ~20 active sources through simultaneous measurements over a frequency range of 1.4–90 GHz. In part, this program was motivated by earlier theoretical work (Jones and O'Dell 1977*a*, *b*) which showed how the internal composition and magnetic structure determined the dependence of polarization on observed frequency through absorption and birefringence (e.g., Faraday rotation). It was also hoped that this new look at compact sources would itself motivate further theoretical work.

Some early polarization measurements from this program were reported in Rudnick *et al.* (1978), and a summary of four sessions of total flux density observations appear in Jones *et al.* (1981). Total flux density results for the fifth and sixth sessions and a summary of all polarization observations appear in Rudnick *et al.* (1985).

In the present paper, we have two main objectives. The first is to address a series of empirical questions, such as: Is there a characteristic pattern to the polarization behavior as a function of observing frequency? Is there any relation to VLBI structures? Our second goal is to synthesize the answers to these questions into a physical picture of compact sources which could then be verified by future observations and complement theoretical investigations.

II. OBSERVATIONS

a) Source Selection

The sources upon which this analysis is based constitute a biased set, chosen primarily for their detectability. The primary data set includes observations at roughly 6 month intervals from 1977 November to 1980 July. We observed ~30–40 strong (> 1–2 Jy) sources with flat or rising spectra ($\alpha > -0.5$; $S \propto \nu^{\alpha}$) per session at centimeter wavelengths. We then chose a smaller set of sources to observe at millimeter wavelengths, based upon their current strength at each epoch and, to a lesser extent, upon whether they seemed likely to have fractional polarizations large enough to be detected at high frequency. These sensitivity considerations may introduce unknown biases into the data sample, so that one should be cautious in extending our conclusions beyond the current data base.

b) Summary of Observing Parameters

Table 1 provides an overview of the multifrequency observations. The session numbers each refer to a distinct observing epoch.

TABLE 1
SUMMARY OF OBSERVING PARAMETERS

Session	Band	Instrument[a]	Dates
1............	11.1 cm, 3.7 cm	GB	1977 Nov–Dec
	6.1 cm, 2 cm	UMRAO	
	9.5 mm	36 foot	
	3.3 mm	36 foot	
2............	11.1 cm, 3.7 cm	GB	1978 Apr–May
	6.1 cm, 2 cm	UMRAO	
	9.5, 3.3 mm	36 foot	
3............	6 cm, 2 cm	VLA	1978 Nov
	3.7 cm	UMRAO	
	3.3 mm	36 foot	
4............	6 cm, 2 cm	VLA	1979 Apr–May
	3.7 cm	UMRAO	
	3.3 mm	36 foot	
5............	6.1 cm, 3.7 cm, 2 cm	UMRAO	1979 Oct–Nov
	3.3 mm	36 foot	
6............	20 cm, 6 cm, 2 cm, 1.3 cm	VLA	1980 July

[a] GB, Green Bank three element interferometer; VLA, Very Large Array; 36 foot, 10.6 m millimeter-wave telescope on Kitt Peak. These facilities are those of the National Radio Astronomy Observatory, operated by Associated Universities, Inc., under contract with the National Science Foundation. UMRAO, University of Michigan Radio Astronomy Observatory, supported in part by the National Science Foundation.

[1] Department of Astronomy, University of Minnesota.
[2] Department of Astronomy, University of Michigan.

III. DISCUSSION

We have only limited direct data about compact radio structures because of their small size. Those data indicate a range of often complex structures and suggest that we are observing a mixture of transparent and opaque regions (e.g., Unwin *et al.* 1982) which depends upon frequency. In addition, the fluxes and structures are time variable. Since polarization is influenced by synchrotron opacity, these characteristics complicate efforts to use linear polarization as a probe of magnetic field structure as has been done in extended sources.

Furthermore, the observed polarization will often be modified by Faraday rotation within the Galaxy or the plasma near the source, and that effect must be removed. Considerable care is required, however, because real magnetic field structures, combined with the effects of the previous paragraph, may mimic or confuse real Faraday rotation behavior. For example, our observations at 1.3 cm and 2 cm show a median position angle difference of 6° between these wavelengths. The observed differences reflect intrinsic, magnetic field structures, as shown by Rudnick and Jones (1983). Therefore, to determine Faraday rotation measures, we used simultaneous polarimetry on the VLA at 18 cm and 20 cm to determine rotation measures for most of the sources discussed in this paper. These wavelengths are long enough and close enough together that measured differences in polarization should be dominated by Faraday rotation rather than magnetic field structures or opacity changes. Rotation measures from that work are reported elsewhere (Rudnick and Jones 1983; Rudnick *et al.* 1984). Rotation measures affecting these sources are typically ~ 50 rad m^{-2} (but with some as large as ~ 300 rad m^{-2}) and time invariant. We believe they are generally galactic in origin. *The data presentations which follow have been corrected for Faraday rotation according to these measurements.*

a) Wavelength Dependence of Polarization

Figure 1 is a synopsis of the polarimetry in the current study. All significant measurements listed in Rudnick *et al.* (1985) are included, provided that at least three wavelengths including 6 cm were available for a given source at a given epoch. Figure 1*a* is a plot of the polarization position angle, χ, at wavelength λ, relative to that at 6 cm, both corrected for Faraday rotation. To facilitate recognition of any systematic wavelength trends in χ for the sample, the sign of $\chi_\lambda - \chi_6$ in Figure 1*a* is chosen for each set of observations so that the accompanying $\chi_2 - \chi_6$ is positive. Although adjacent observing bands separated by a factor 2–3 in wavelength differ in position angle typically by $\lesssim 20°$, there is no systematic wavelength trend evident in Figure 1*a*. The positive definition of $\chi_2 - \chi_6$ creates a $\sim 10°$ offset for $\nu > 5$ GHz, but otherwise the sources generally seem to exhibit individual wavelength-independent characteristic position angles accompanied by considerable scatter. The band-to-band differences generally exceed measurement uncertainties and, therefore, represent real wavelength dependence. If one connects the data points for individual sources in Figure 1*a*, the overall impression is one of randomness for most of the sources.

Figure 1*b* plots, from the same measurements as Figure 1*a*, the degree of polarization (corrected for error bias) normalized to the value seen at 6 cm for a given source and epoch. There is clearly a great deal of scatter in m_λ/m_6 even for adjacent wavelengths. On the other hand, the median value of m_λ/m_6 at each λ is unity to within 20%. Thus there is on average no depolarization toward long wavelengths, which could be attributed (1) to internal Faraday depolarization (cf., e.g., Jones and O'Dell 1977*a*), (2) to decreased dominance of relatively unpolarized opaque regions (e.g., Jones and O'Dell 1977*a*, *b*; Jones and Hardee 1979), or (3) to increased magnetic field ordering on the smaller-scale regions dominating the shorter-wavelength emissions. The median value of m_6 is $\sim 2.5\%$ (see also Rudnick and Jones 1982). Again, when the data points of each individual source are connected together, the impression is one of randomness for most sources.

To examine more fully the scatter evident in Figure 1*a*, it is useful to plot the Stokes parameters $Q = P \cos 2\chi$ and

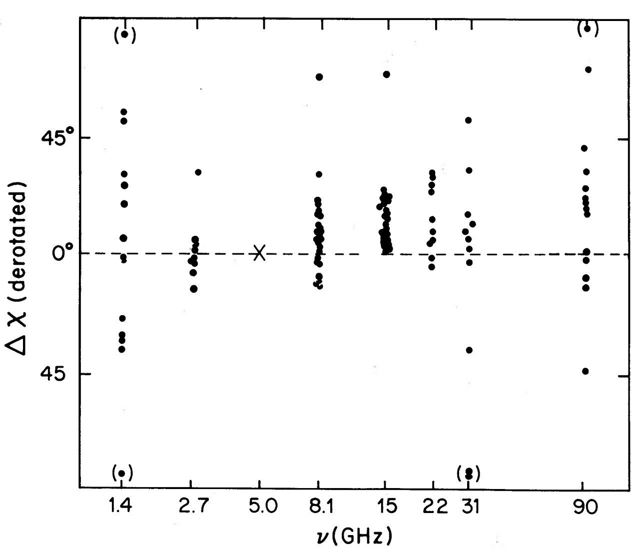

FIG. 1*a*

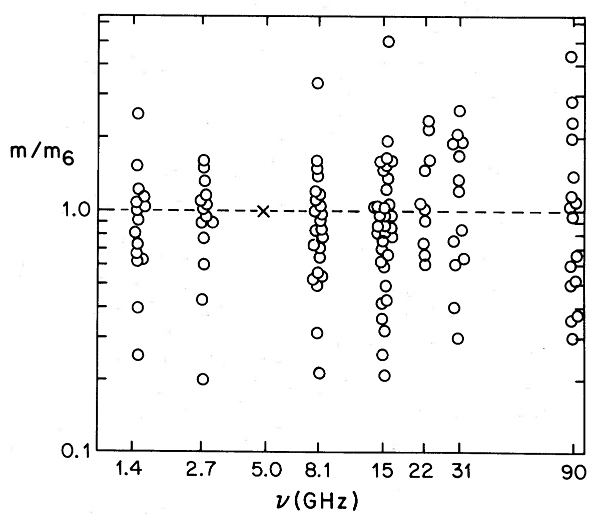

FIG. 1*b*

FIG. 1.—(*a*) Polarization position angle relative to 6 cm after correction for Faraday rotation. Value at 2 cm is defined as positive definite (setting the sign convention for other wavelengths at that epoch) to facilitate identification of monotonic trends. Each point represents a measurement simultaneous with one at 6 cm. (*b*) Degree of polarization relative to 6 cm. Each point represents a measurement simultaneous with one at 6 cm.

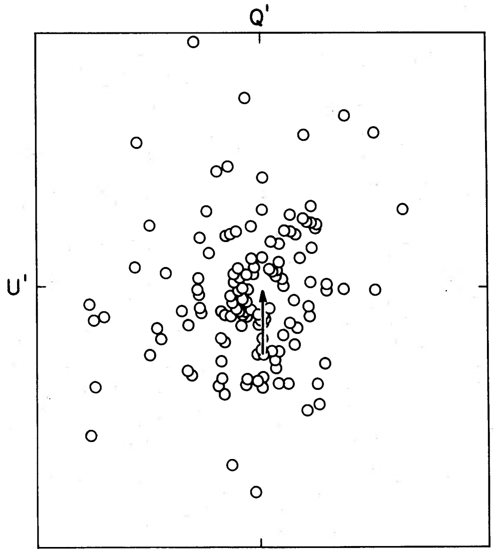

FIG. 2.—Stokes vector (Q, U) diagram of polarization around the 6 cm Stokes vector. Arrow represents a 2% 6 cm Stokes vector.

$U = P \sin 2\chi$. The quantity (Q, U), which we shall call the Stokes vector, obeys vector arithmetic. We can therefore attempt to separate a Stokes vector into various contributing elements, such as a wavelength-independent, or what we shall call a "common," component and a residual random component, for example.

We can explore this problem through Figure 2, which is a replot of the data in Figure 1 in terms of the normalized Stokes vector $(Q, U)/I = (q, u) = m(\cos 2\chi, \sin 2\chi)$. For each point we have subtracted the associated polarization vector at 6 cm from that at the plotted wavelength. In addition, the coordinate system is rotated so that $\chi_{6\text{ cm}} = 0$ for each source and epoch. The resulting plot is of the Stokes vector difference between λ and 6 cm in directions relative to the 6 cm polarization. The distribution in Figure 2 is roughly isotropic about the origin, with dispersions $\sigma_q \approx 2.7\%$ and $\sigma_u \approx 2.5\%$. It also approximates a Rayleigh distribution $\sim(r/\sigma) \exp - (r^2/\sigma^2)$, which would be the result, for example, if each point in Figure 2 were the endpoint of a vector from the origin which was the sum of several elements of random phase (Rayleigh 1880).

Since there is nothing unique about 6 cm except that it was almost always present in our data, the random pattern in Figure 2 is most easily interpreted as evidence for the presence of a random component to the polarization, m_r, which is typically $\sim$2.5% at all wavelengths. However, since the typical value of $m_6 \sim 2.5\%$, as well, the actual distribution of Stokes vectors in a typical source is offset from the origin (see Fig. 3, for example). This accounts for the patterns seen in Figure 1. We can attribute the offset to a common polarization component (defined two paragraphs above). We will use the median Stokes vector for each source and epoch as an estimator of the common Stokes vector. Its typical length is $m_c \sim$ 2.5%. This result is statistical in nature but is also consistent with Stokes vector plots of a number of individual sources. For example, Figure 3 illustrates the Stokes vectors of 0355+50 at session 2. These data scatter around a vector $\sim(-1.5, 0)\%$. As we shall see below, however, not all sources completely fit this description (see Fig. 7, for example).

b) *Magnetic Field Structures*

i) *Degree of Order*

The polarization is a signature of the magnetic field structure within a source. To model that field from the above polarization behavior, we will take our statistical results to represent a typical source. To construct a simple phenomenological model we first recall that since compact sources are partially opaque (e.g., Kellermann and Pauliny-Toth 1981), we sample different emitting volumes at different observed wavelengths. Hence, the random scatter in polarization reflects a magnetic field whose net projected direction varies in a partially random way with source position; i.e., the field is turbulent. In this typical source the projected field is not completely random, however, but has a well-defined direction imprinted on it as well. That is to say, the turbulence is anisotropic. The anisotropy could result, for example, from shear or compression in a fluid with near frozen-in field or from large-scale current systems in the source. It is important to evaluate both the degree to which the source is ordered and the spatial scale of the disorder and in addition to determine the orientation of the asymmetry in the magnetic field structure. These three data provide clues about the origin of the field, about its evolution within the source structure, and about such important matters as particle acceleration.

We will begin by trying to establish the degree to which the field is disordered. To this end we have generalized a statistical field model discussed by Laing (1980). He considered a field which was compressed into a plane, its distribution in the plane being isotropic. We have considered a magnetic field structure which is statistically also uniformly distributed in azimuth around a symmetry axis, or pole, but which in addition is uniformly distributed over a finite range of latitudes, θ, bounded by a value Θ. The average polarization degree then depends upon the range of Θ available to the field and upon the orientation of the polar axis. The polarization of a particular source region would scatter around this value with an amplitude that depends upon the scale of the field disorder, i.e., upon the number of spatially independent field orientations.

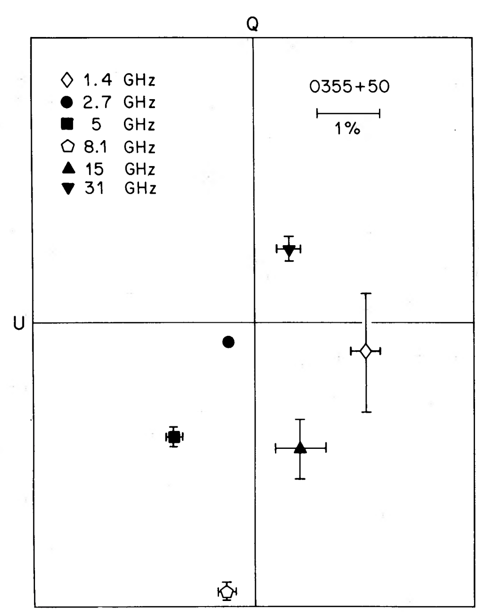

FIG. 3.—Stokes vector (Q, U) diagram of the polarization of 0355+50 (NRAO 150).

Two model cases of interest are for distributions $\theta \leq \Theta \leq \pi/2$ (which reduces to Laing's model as $\Theta \rightarrow 0$) and $\Theta \leq \theta \leq \pi/2$. The former case we will refer to as transverse compressed symmetry (TCS) and the latter as aligned symmetry (AS). For transverse compressed symmetry the mean polarization vector (E) is aligned with the projected polar direction, whereas for axial symmetry the mean polarization direction is perpendicular to the projected polar direction. The mean degree of polarization, which we identify with m_c (the common polarization), will depend in each case upon the viewer's latitude, β_S, as well as Θ. As in Laing's calculation we can take the analytic formulae derived from unit spectral index synchrotron emissivity as representative. We have

$$m_c = m_0 \frac{\cos^2 \Theta \cos^2 \beta_S}{1 + \sin^2 \beta_S + \sin \Theta(\cos^2 \beta_S - 2/3)} \quad \text{(TCS)},$$

$$m_c = m_0 \frac{\cos^2 \Theta \sin \Theta \cos^2 \beta_S}{4/3 - \sin \Theta(1 + \sin^2 \beta_S) - \sin^3 \Theta(\cos^2 \beta_S - 2/3)} \quad \text{(AS)}, \qquad (1)$$

where $m_0 \sim 0.7$ is the intrinsic degree of polarization. This model is intended as a convenient way of emulating a range of plausible field configurations rather than as an accurate physical description of the field structure.

In this model the $\sim$2%–3% common polarization of our typical source would reflect both the degree of anisotropy, measured through Θ, and the projection angle β_S. To first order, we can ignore complications introduced by flux contributions from opaque regions, by assuming them to be unpolarized. As an example, let us assume they contribute roughly half the total flux, leading to a net 4%–6% common polarization (and a comparable superposed random polarization) from transparent regions. If the sources we observe are uniformly oriented in space, the majority has $|\beta_S| < 60°$. In that event, to produce a common $m_c \sim$ 4%–6%, a field such as that represented in equations (1) must be reasonably isotropic; namely, we must have $\Theta > 75°$ (TCS) or $\Theta < 5°$ (AS). In more common form, this result can be stated roughly as $\Delta B^2/B^2 = |\langle B_\perp{}^2 \rangle - \langle B_\parallel{}^2 \rangle| / (\langle B_\perp{}^2 \rangle + \langle B_\parallel{}^2 \rangle) \lesssim 5\%$. Available VLBI observations indicate that when unpolarized structures are removed, values of $m \sim 30\%$ are sometimes found (Cotton, Geldzahler, and Shapiro 1982; Wardle 1984). If we separate this into superposed common and random vectors, we are left with common polarizations, $m_c \sim 20\%$. This would lead in our magnetic model to $\Theta \gtrsim 60°$ (TCS), $\Theta \lesssim 15°$ (AS), $\Delta B^2/B \lesssim$ 15%–20%.

If sources are relativistically beamed, those directed toward the observer will then be preferentially selected in flux-limited samples (e.g., Scheuer and Readhead 1979). It might seem at first glance that this would give a large preference to values of $\beta_S \sim \pi/2$ in equations (1), provided the kinematic and magnetic symmetry axes are aligned. However, equations (1) are cast in terms of the viewing angle *in a frame comoving with the emitting material*, so one must correct for aberration to estimate the distribution of β_S in this situation. Take, for example, jetlike sources with flat spectra. They will have their fluxes Doppler boosted by a factor proportional to $D^2 = (1 + v/c \sin \beta_K)^2$, where β_K is the comoving latitude in the kinematic system (e.g., Blandford and Königl 1979). In a flux-limited sample drawn from sources with a uniform space density, the detection probability per unit laboratory solid angle will then be enhanced by a factor D^3, since the limiting distance varies as D. But the solid angle over which the enhancement holds is reduced through relativistic beaming by a factor D^{-2}. Since $d\Omega \propto \cos \beta_K \, d\beta_K$, the probability distribution per unit β_K will have the form $\cos \beta_K(1 + v/c \sin \beta_K)$, which is only moderately forward peaked even as $v \rightarrow c$ (broadly peaking at $\beta_K = 30°$ for $v = c$). This conclusion is of general importance; *in flux-limited samples, the distribution of comoving viewing angles is broad even when* $v \rightarrow c$.

Consequently, the interpretation of our data in terms of equations (1) is not significantly different from the nonrelativistic result in the previous paragraph. We conclude that even with relativistic beaming included, the magnetic field in our typical source is largely turbulent and almost, but not quite, isotropic. Furthermore, much of the variation in relative polarization ordering from source to source can probably be explained through variations in viewing angle rather than just intrinsic differences in the magnetic structures.

Next we need to estimate the spatial scale of the magnetic field disorder. This we can determine from the amplitude of the scatter in the polarization around the common vector. The observed scatter with wavelength of the polarization, m_r, from our typical source around its mean vector has an amplitude comparable to the common polarization vector ($m_r \sim$ 2%–3%, as measured from integrated measurements). Since we determined in the preceding paragraphs that the magnetic field is roughly isotropic, we may model the polarized flux at a given wavelength as coming from N statistically independent regions. If a fraction f_u of the integrated flux comes from unpolarized regions, the expected polarization scatter around the mean, which we identify with m_r, is $m_r \sim (1 - f_u)m_0/N^{1/2}$. With $m_r \sim 2.5\%$ and $f_u \sim 0.5$, one obtains $N \sim 200$ implying a turbulence scale length $R_t = N^{-1/3}R \sim 0.2R$, with R the source size. If $f_u \sim 0.9$, so that the measured m_r corrected for unpolarized regions is $\sim$25%, then $N \sim 10$ and $R_t \sim 0.5R$. The statistical model becomes less accurate in that regime, of course.

ii) *Orientation of Ordered Field*

The relative orientation of the polarization to the source structural axis is also important. Analyses of extended radio jets have tended to find a bimodal distribution indicating that the field is either nearly aligned with the structural (and kinematic) axis or orthogonal to it (e.g., Bridle 1982). There are some indications in extended jets that the field structure also evolves from a parallel to an orthogonal alignment with increasing distance from the source core (e.g., Bridle 1982). A luminosity dependence in magnetic orientation has also been seen (e.g., Clarke, Kronberg, and Simard-Normandin 1980). Previous attempts to explore these questions for compact sources have met with less success. Altschuler and Wardle (1977) found no evident relationship. Davis, Stennard, and Conway (1978) considered three sources 3C 273, 3C 345, and 3C 454.3 and concluded that the magnetic fields were misaligned by about 20° from the source major axis, and that in 3C 273 and 3C 345 the field direction curved to follow the bending source axis. The latter conclusion is incorrect at high frequencies, as shown in Figure 4.

These earlier studies of compact sources were hampered by insufficient data and an inadequate knowledge of Faraday corrections and irregularities in the magnetic field. Furthermore, projection effects can also mask field-source structural relations. Blandford and Königl (1979) have emphasized, for example, how misalignment and relativistic aberration can

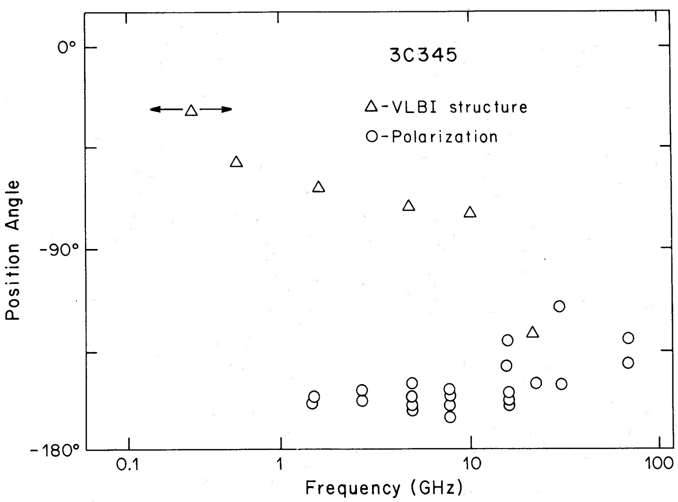

FIG. 4.—Polarization angles and structural major axis angles for 3C 345

combine to give wide-ranging polarization angles relative to the kinematic axis.

Consequently, we need to look carefully at projection effects when the magnetic and kinematic axes are misaligned. As in § III*b*(i), let the complement to the angle between the line of sight and kinematic axis (the latitude) be β_K. If the magnetic field symmetry axis has polar and azimuthal angles α and ϕ in the kinematic coordinate system (see Fig. 5), then the projected angle on the sky between the kinematic axis and the field symmetry axis, δ, satisfies

$$\tan \delta = \frac{\sin \alpha \cos \phi}{\cos \alpha \cos \beta_K + \sin \alpha \sin \beta_K \sin \phi} . \quad (2)$$

As in the earlier discussion all of these angles are referred to the comoving frame. From equation (2) it is clearly not possible to determine uniquely the misalignment, α, for an individual source. However, when the viewer's polar angle $(\pi/2 - \beta_K)$ is large $(>\alpha)$, δ remains in one quadrant and has a well-defined average as ϕ varies from 0 to π. We shall see below that making this assumption leads to a self-consistent result. Thus, although one cannot confidently determine the misalignment α for a single case, a straightforward integration of equation (2) yields the average result from an ensemble

$$\tan \alpha = (\cot \beta_K) \frac{\exp (\pi\langle \tan \delta \rangle \sin \beta_K) - 1}{\exp (\pi\langle \tan \delta \rangle \sin \beta_K) + 1} , \quad (3)$$

where $\langle \tan \delta \rangle$ is averaged over ϕ. As $\beta_K \to 0$, this reduces to $\tan \alpha = (\pi/2)\langle \tan \delta \rangle$. The β_K dependence is fairly flat, except as $\beta_K \to \pi/2$. Since we argued before that (even after correction for aberration) the majority of our sources probably have $|\beta_K| < 60°$, we conclude that $\alpha \sim \langle \delta \rangle$ is a good estimate. In terms of the magnetic field model discussed above, the difference between the common polarization angle and the source kinematic (major) axis, $\Delta\chi$, is either δ (TCS) or $\pi/2 - \delta$ (AS).

Returning to the observational data of Rudnick *et al.* (1985), the available data bearing on the alignment question are listed in Table 2. Except where noted, the polarization angles are

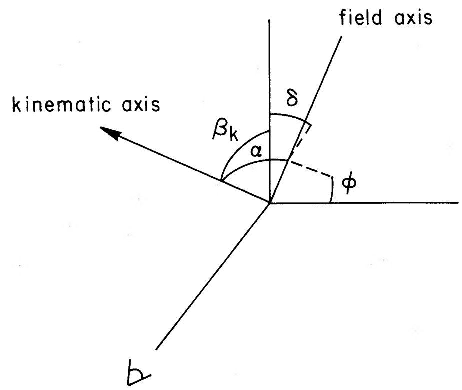

FIG. 5.—Coordinate definitions for discussion of field misalignment projection.

TABLE 2

POLARIZATION AND STRUCTURAL ANGLES

Source[a]	Pol. Angle	Milli-arcsec Major Axis	Ref.	Arcsec Major Axis	Ref.	|Col. (2) − Col. (1)|	|Col. (3) − Col. (1)|	|Col. (3) − Col. (2)|
0007+10	7	...	...	180°	1	...	7	...
0355+50	85	78	2	110	1	7	25	32
0430+05	−15	−108	3	−99	4	87	84	9
0735+17	−55	43	2	170	1	82	45	127
0851+20	0	80	2	80	4	80	80	0
0923+39	83	−125	5	...	...	28	...	...
1055+01	−70[b]	...	...	180	1	...	70	...
1226+02	−23	−99, −138	6	−138	1	76, 65	65	39, 0
1308+32	90	10	7	90	8	80	0	80
1510−08	41[b]	...	...	160	1	...	61	...
1641+39	27	−135, −57	6	−30	1	18, 84	62	105, 27
1749+09	90	−63	9	...	...	27	...	...
2134+00	−20[b]	60	10	...	...	80	...	...
2200+42	85	−170	11	...	...	75	...	...
2223−05	0[b]	90 ± 30	12	−32	...	90	32	122
2251+15	14	−65	13	48	...	79	34	113

[a] The following sources were observed in the program but have inadequate polarization or structural information to be included: 0235+16, 0300+47, 0420−01, 0552+398, 0736+01, 0754+10, 1219+28, 1404+28, 1418+54, 1921−29, 2005+40.

[b] 6 cm or 2 cm, uncorrected for Faraday rotation. All other entries have been corrected.

REFERENCES.—(1) Perley 1982. (2) Bååth *et al.* 1980. (3) Walker *et al.* 1982. (4) Browne *et al.* 1982*a*. (5) D. B. Shaffer, private communication. (6) Readhead *et al.* 1983. (7) Weiler and Johnston 1980. (8) Rudnick and Jones 1983. (9) L. Bååth, private communication. (10) Pauliny-Toth *et al.* 1981 (11) Phillips and Mutel 1982. (12) R. L. Brown, private communication. (13) Cotton, Geldzahler, and Shapiro 1982.

median values derived from all of our data on a given source. By combining the (n) polarization measurements we can expect, according to the above interpretation, to reduce the uncertainty in the characteristic χ from $\sim 30°$ for an individual measurement by a factor $\sim 1/n^{1/2}$ to 10°–15° in most cases. The sources of structural orientation data are cited in the table. Two structural orientation values have been listed for each of the bent sources, 3C 273 and 3C 345. These represent the range of observed angles. Histograms of the values of $|\Delta\chi|$ relative to milli-arcsec structure and arcsec structure are given in Figure 6. Again two values each are included for 3C 273 and 3C 345.

It is clear that the large majority of the sources are consistent with aligned symmetry (AS) field structures with relatively small misalignments from the milli-arcsec structure. Uncertainties in structural and median polarization angles may very well account for most of the apparent scatter around perfect alignment. Our sources, therefore, are similar for the most part to extended jets which show the field to be axial nearest their cores. It should be noted, however, that the cores of the larger structures are different in several ways from the sources studied here. Our own analysis of the cores of extended sources shows them to be largely unpolarized (Rudnick and Jones 1985). We should note that the pattern in Figure 6 (*top*) is not evident

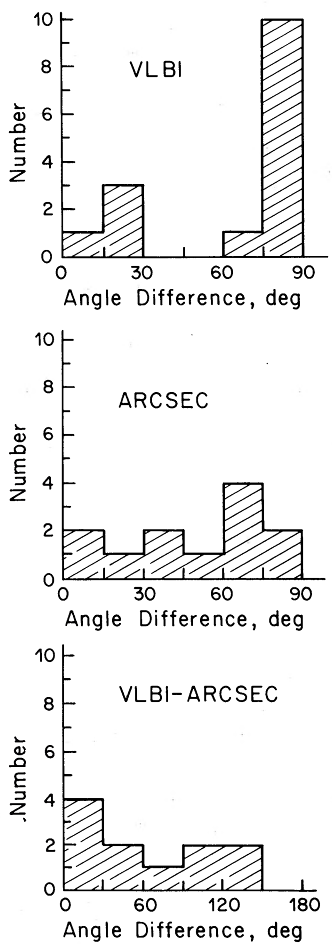

FIG. 6.—Histograms of (*top*) common polarization (defined in text) relative to milli-arcsec major axis, (*middle*) common polarization angle relative to arcsec structural major axis, and (*bottom*) milli-arcsec major axis relative to arcsec major axis.

when one uses individual polarization scatter which we discussed above.

Four of our sources appear from Figure 6 to be consistent with transverse compressed symmetry (TCS). They are 0851+20 (OJ 287), 0355+50 (NRAO 150), 1749+09, and the smallest-scale structure in 3C 345. Note, however, that the spectrum of NRAO 150 (see Table 2 or Jones *et al.* 1981) showed signs of a self-absorption turnover at wavelengths longer than 2 cm. The highest-frequency polarization (31 GHz) was roughly orthogonal to the others, possibly indicating influence from synchrotron self-absorption at the lower frequencies (see Fig. 3, however). In that case NRAO 150 would also indicate AS field structure. Likewise, 1749+09, had a spectrum which was strongly inverted (Table 2), suggesting that it, too, may have been significantly self-absorbed. We will further discuss NRAO 150, 1749+09, and 3C 345 below in conjunction with 3C 454.3, which may exhibit related characteristics.

It is interesting that OJ 287 apparently falls into the small-$\Delta\chi$ (TCS) category because this source has shown the highest known polarization, and its polarization direction is uncommonly steady in both time and wavelength, including visual wavelengths (Rudnick *et al.* 1978). Given those characteristics it is not plausible that the OJ 287 polarization angle is modified by self-absorption. Consequently we conclude that this source actually has a TCS magnetic field structure. It may be worth noting that BL Lac also seems to develop TCS fields during some outbursts (Aller, Hodge, and Aller, 1983; Phillips and Mutel 1982), perhaps as a result of shock compression of the magnetic field.

The relationship between the polarization (which variability shows is largely due to sub-arcsec structure) and the arcsec structure is not as well defined. In fact the relative orientations of the arcsec and milli-arcsec structures of the sources in Table 2 are very broadly distributed, also shown in Figure 6. This presumably reflects curvature in several cases (e.g., Readhead *et al.* 1983; Browne *et al.* 1982*b*).

A statistical model neglecting radiative transfer effects (see, e.g., Jones and O'Dell 1977*a*, *b* for a summary of such effects) and with at most one "common," or preferred, direction is too simple, of course, to explain completely every source. Some sources show clear, systematic wavelength trends in their polarizations. A good example is 2251+15 (3C 454.3). Figures 7*a* and 7*b* show position angle and Stokes vector plots, respectively, for this source. It is clear from Figure 7*b* that the trend in χ is not a rotation, but that there is a null and $\sim 90°$ flip in the polarization between 2 cm and 3 cm. The spectrum of the source was complex and slightly inverted during this time (Table 2; Jones *et al.* 1981). Cotton, Geldzahler, and Shapiro (1982) have published a 13 cm VLBI polarization map of this source which (with our Faraday rotation measure) shows the position angle in the "core" to be similar to what we observe at high frequencies, while that in the "jet" is similar to what we observe at low frequencies. One can interpret all of these data together in terms of a change in the projected net magnetic field direction from TCS magnetic field structure in a small core to AS in the large-scale jet (e.g., Komesaroff *et al.* 1984), or in terms of an increased dominance at high frequencies of emission from an opaque core.

3C 345 shows some of the same characteristics as 3C 454.3 if in 3C 345 one projects the polarization against the curving source axis. However, in 3C 345 there is no clear polarization null, such as that exhibited by 3C 454.3. NRAO 150 may also

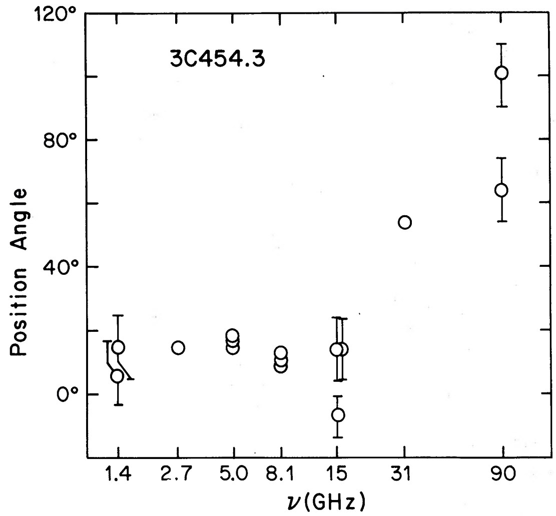

FIG. 7a

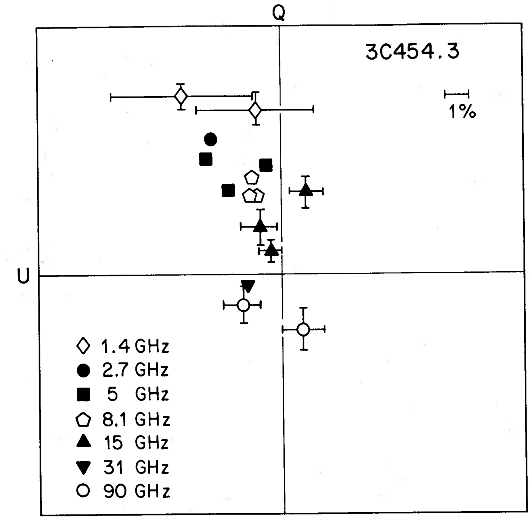

FIG. 7b

FIG. 7.—(*a*) Position angles in 3C 454.3 as a function of observing frequency. (*b*) Stokes vector (Q, U) diagram of the polarization of 3C 454.3.

have exhibited a 90° flip, but in the opposite sense to 3C 454.3. We have not observed the polarization of 1749+09 above its spectral turnover, so we can only speculate that it, too, may have been affected by self-absorption.

c) Time Dependence of Polarization

i) *Evidence for Random Behavior*

If the source magnetic fields consist largely of random elements, then because these elements should evolve in time, we may expect evidence of this in polarization time variations as well as in wavelength dependence. Our broad-band program has inadequate time coverage to detect this, but we can examine the extensive University of Michigan polarization monitoring results of the same sources in the same time period. The 3.75 cm (8 GHz) data are the most complete and highest quality, so we concentrate here on those.

Many of the time changes present in our data can be understood in terms of random fluctuations of Stokes vectors around a relatively steady component. Moore *et al.* (1982) have interpreted detailed optical polarization observations of BL Lac in a similar way. They demonstrated that the power spectrum of polarization changes in BL Lac was that of a random walk. Our data are too incomplete for that type of analysis, but we can visually examine Stokes vector diagrams of the 3.7 cm data.

Figure 8 shows the path of the 3.7 cm Stokes vector of BL Lac during 1976–1980. Each vertex represents the polarization averaged over a month. These data are from a relatively inactive period of one of the more variable sources in our sample. This diagram is fairly representative of the other sources as well. For our sources as a whole, the dispersion of the Stokes vector around the median point (in time) averages ~2%, comparable to the value found for wavelength-dependent scatter at a single epoch. One can do a similar analysis of the Altschuler and Wardle (1976) data base with like results. On the whole, the scatter is fairly isotropic, as it was in wavelength, but individual sources do sometimes show asymmetries (see, e.g., Aller, Olson, and Aller 1976). In many models an estimate of the expected time scale for polarization variations is simply the time required to replace the polarized emitting volume. In jetlike models this will be comparable to or a bit less than that for flux changes. Wavelength correlation of polarization time changes should be comparable to the instantaneous correlation in wavelength (as indicated in Fig. 1). Both of these expectations are borne out by the data, as is the expectation that many polarization changes are uncorrelated with flux changes. There are, of course, cases where the effective opacity and/or the field structure appear to change substantially during outbursts (e.g., in BL Lac; Aller, Aller, and Hodge 1981).

ii) *Polarization "Rotators"*

By examining Stokes vector diagrams one can identify occasional events in which the Stokes vector appears to execute a complete rotation around the origin. Several such events involving apparent rotations around the origin have been reported (Ledden and Aller 1978; Aller, Hodge, and Aller

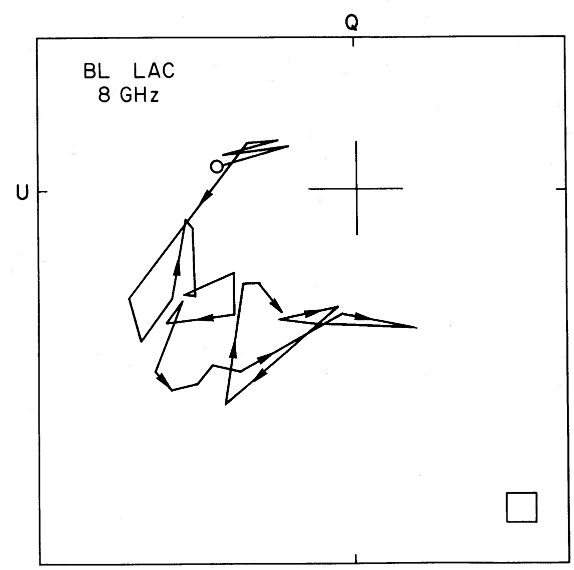

FIG. 8.—Stokes vector (Q, U) diagram of the 8 GHz polarization of BL Lac from 1976 April to 1978 October. Plus indicates origin, with each arm extending 2% each day. Box gives typical error.

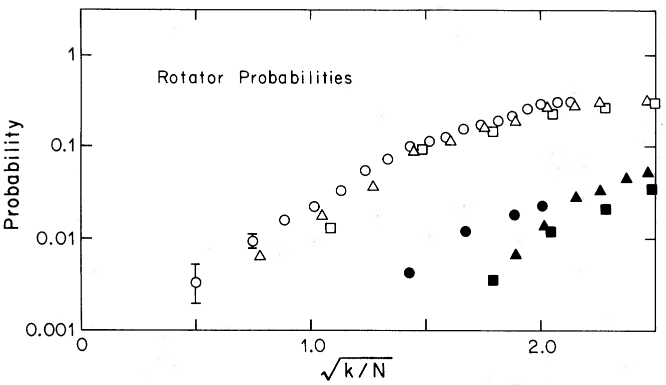

FIG. 9.—Probability of random 2π and 4π Stokes vector rotations as described in the text. Open symbols refer to 2π events; filled symbols to 4π events. Boxes correspond to $N = 5$, triangles to $N = 10$, circles to $N = 20$. N is the number of independent elements in each random vector, while k is the number of the time step. Sample error bars indicate statistical uncertainties for various probability levels.

1981; Altschuler 1982). These events have come to be known as "polarization rotators." The interpretation of rotators has been in terms of rotating bodies (Aller, Hodge, and Aller 1981) or aberration effects (Blandford and Königl 1979). But in view of the results in this paper, an alternative explanation may be in terms of random variations in the magnetic field. In all reported rotator events, the value of m was relatively small ($<2\%$) during the event. Thus they may be associated with times when the common Stokes vector (defined in § IIIb) is small or absent. Then, random walks around a closed path can appear as rotations about the origin.

Is it reasonable to expect a significant number of rotators in a random process? To answer this question we performed Monte Carlo calculations using a simple two-dimensional polarization model. An initial Stokes vector was constructed of N two-dimensional time-dependent unit vectors with random phase (orientation).[3] (Hence, the origin was set at what would be the tip of any common Stokes vector present.) Then at each time step, k ($k \geq 1$), a new random unit vector, labeled $(N + k)$ was added, while the kth unit vector was subtracted, keeping N constant. Maintaining the number of components, N, as a constant is appropriate on average since the rms length ($\propto N^{1/2}$) of observed polarization vectors is not a monotonic function of time. Furthermore, simple models such as a steady jet convecting a turbulent field into view would have this property. For each experiment we monitored the length and phase of the resultant vector as a function of time. From all experiments we then computed the probability[4] as a function of k and N that the algebraic phase change in the Stokes vector after k steps exceeded 2π radians or 4π radians (an integrated change in polarization angle of at least 180° or 360° respectively). Figure 9 summarizes the results for N from 5 to 20. Each point represents 3200 experiments. As the number of time steps, k, exceeds N (as the average summed length of the "added" vectors exceeds the average length of the initial N component vector), the probability of a 2π rotation increases rapidly, leveling off to $\sim 30\%$ for $k \gtrsim 3N$. We verified visually for successful rotations with $k \sim N$ that the Stokes vector typically followed a path resembling an orderly rotation, i.e., that the position angle increases approximately linearly with time. (One expects for $k \gg N$ to obtain formal successes which would not appear as rotations if examined visually.) Figures 10a and 10b compare an example of one of these Monte Carlo events with the rotation in BL Lac reported by Aller, Hodge, and Aller (1981). Figure 9 also illustrates the probability of a 4π rotation, which appears to be about 10 times smaller than for 2π. These outcomes are indeed plausible when one considers that the

[3] We performed analogous calculations in which the Q and U were uniformly distributed in the interval $[-1, 1]$ for each of the component vectors. Results were almost identical.

[4] Defined as the ratio of the number of successful trials to total experiments.

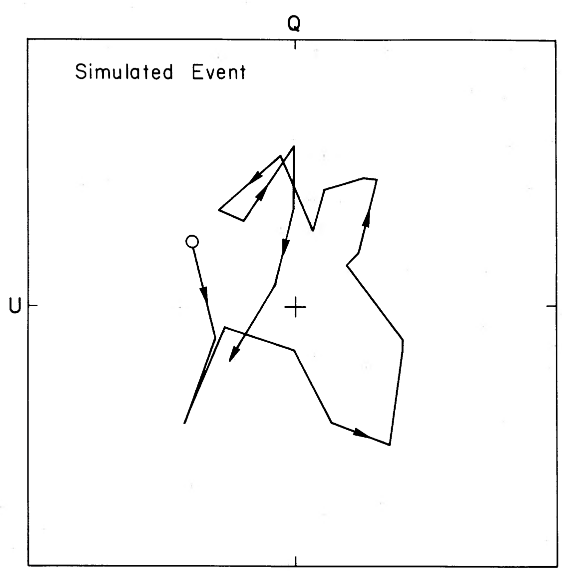

FIG. 10a

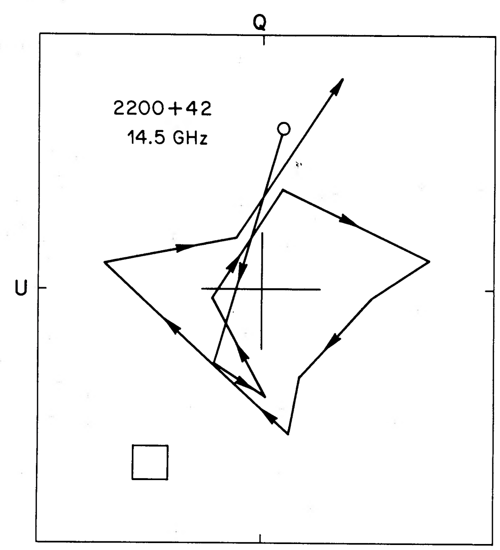

FIG. 10b

FIG. 10.—(a) Random walk simulation of a rotator event as seen in the Q-U plane. In this example $N = 10$. (b) Polarization rotator event of BL Lac at 15 GHz during 1980 May and June. Vertices (measurements) are separated by an average of about 5 days. Plus indicates origin, with arms extending 1% each way. Box gives typical error.

endpoint distribution for the individual vectors (the Rayleigh distribution) is concentrated in an annulus. Therefore, the vector is most likely to wander within the annulus, occasionally circulating around it.

We conclude, therefore, that the polarization rotator events reported thus far could very well be understood as a random process, although this does not constitute proof. If this is indeed correct, then Figure 9 suggests that more thorough observations would turn up such events fairly frequently, especially if one looked for rotations around points offset from the origin. According to this hypothesis, position angle rotations of both signs should occur with roughly equal frequency in a given object. With short–time scale monitoring, as achieved on several objects by Aller, Aller, and Hodge (1981), this empirical model could be used to identify a characteristic time scale for independent components, and the number of individual components in a source, since as N beomes small, the individual characteristic shifts in the Q-U plane beome large.

We should point out that there are also examples in the literature of systematic transitions in the polarization properties. For example, O'Dea *et al.* (1983) and Komesaroff *et al.* (1984) report in 1308+32 a $\sim 90°$ shift in the position angle during 1977 at 6 cm. That took the 6 cm position angle from a value near the one observed by us at 11 cm and 20 cm to a value observed by us at several shorter wavelengths. Other such events have also been published (e.g., Aller, Aller, and Hodge 1981). These may well represent opacity-related transitions in certain simple objects, such as those we discussed for the simultaneous broad-band data on several sources.

IV. CONCLUSIONS

From this work we can draw several important conclusions about the polarization and magnetic field structures in active compact radio sources. Most of these results could not have been obtained without very broad band measurements. (See Jones *et al.* 1981 for a discussion of broad-band spectral characteristics, and Rudnick and Jones 1982 for a comparison of polarization properties among various classes of compact sources.) Some of the conclusions which stand out in the present work are the following:

1. The degree of polarization in our sample is generally not a monotonic function of wavelength, either in individual sources or for the sources as a whole. The median polarization of the sample remains $\sim 2.5\%$ over almost two decades in frequency. This is true despite large variations in the degree of polarization from wavelength to wavelength in a given source.

2. After correction for Faraday rotation, most of the sources show polarization angles, at different wavelengths and times, that scatter around a "common" value. On the other hand, there are a few clear examples of systematic trends which may suggest self-absorption effects. For those sources which have measured VLBI structures, the structural major axis is usually nearly orthogonal to the common polarization ($\boldsymbol{E}$) direction; i.e., the magnetic fields tend to be parallel to the VLBI axis.

3. Even rather close wavelengths exhibit considerable scatter in their polarization position angles. The median 1.3–2 cm scatter is 6°; for 2–6 cm it is 20°. These intrinsic differences are large enough that in order to determine Faraday rotation corrections, it is important to use simultaneous measurements which are very closely spaced in wavelength.

4. When the polarization is displayed in terms of normalized Stokes parameters Q/I and U/I, it shows a random, nearly isotropic scatter around a "common" Stokes vector. Thus the polarization apparently can be decomposed into a wavelength-independent, or common, vector component and a random vector component. In a typical source the observed lengths of the common vector and the rms random vector are comparable, $\sim 2\%$–3%.

5. This behavior is also shown by the time behavior of polarization at 8 GHz. These results together can be understood through a model magnetic field which possesses an anisotropic, but axisymmetric turbulent character. The degree of anisotropy is relatively small ($\Delta B^2/B^2 \sim 5\%$ [15%–20%] if roughly 50% [90%] of the total flux originates from opaque, unpolarized regions), with the preferred field direction aligned with the source kinematic axis in most cases. The dominant scale of the turbulence is $\gtrsim 10\%$ of the source scale size. Monte Carlo simulations based on such a model show that polarization "rotator" events and variations in general may be the natural consequence of the evolution of a random magnetic field.

6. In evaluating the effects of relativistic beaming on the appearance of sources, it is important to realize that the distribution of comoving viewing angles is broad even as $v \rightarrow c$, for sources drawn from a flux-limited sample. Thus, for example, one does not expect to preferentially observe magnetic fields close to the line of sight even if they are well aligned with the source kinematic axis.

This work was supported by the NSF at the University of Minnesota under grants AST 79-00304, AST 81-14737, and AST 83-15949 and at the University of Michigan under grants AST 78-24192 and AST 80-2150.

REFERENCES

Aller, H. D., Aller, M. F., and Hodge, P. E. 1981, *A.J.*, **86**, 325.
Aller, H. D., Hodge, P. E., and Aller, M. F. 1981, *Ap. J.* (*Letters*), **248**, L5.
———. 1983, *Ap. J.* (*Letters*), **274**, L19.
Aller, H. D., Olson, E. T., and Aller, M. F. 1976, *A.J.*, **81**, 738.
Altschuler, D. R. 1982, *A.J.*, **85**, 1559.
Altschuler, D. R., and Wardle, J. F. C. 1976, *Mem. R.A.S.*, **82**, 1.
———. 1977, *M.N.R.A.S.*, **179**, 153.
Bååth, L. B., *et al.* 1980, *Astr. Ap.*, **86**, 364.
Blandford, R. D., and Königl, A. 1979, *Ap. J.*, **232**, 34.
Bridle, A. H. 1982, in *IAU Symposium 97*, *Extragalactic Radio Sources*, ed. D. S. Heeschen and C. M. Wade (Dordrecht: Reidel), p. 121.
Browne, I. W. A., Clark, R. R., Moore, P. K., Muxlow, T. W. B., Wilkinson, P. N., Cohen, M. H., and Porcas, R. W. 1982*a*, *Nature*, **299**, 788.
Browne, I. W. A., Orr, M. J. L., Davis, R. J., Foley, A., Muxlow, T. W. B., and Thomasson, P. 1982*b*, *M.N.R.A.S.*, **198**, 673.
Clarke, J. H., Kronberg, P. P., and Simard-Normandin, M. 1980, *M.N.R.A.S.*, **190**, 205.
Cotton, W. D., Geldzahler, B. J., and Shapiro, I. I. 1982, in *IAU Symposium 97*, *Extragalactic Radio Sources*, ed. D. S. Heeschen and C. M. Wade (Dordrecht: Reidel), p. 301.
Davis, R. J., Stennard, D., and Conway, R. G. 1978, *M.N.R.A.S.*, **185**, 435.
Jones, T. W., and Hardee, P. E. 1979, *Ap. J.*, **228**, 268.
Jones, T. W., and O'Dell, S. L. 1977*a*, *Ap. J.*, **214**, 522.
———. 1977*b*, *Ap. J.*, **215**, 236.
Jones, T. W., Rudnick, L., Owen, F. N., Puschell, J. J., Ennis, D. J., and Werner, M. W. 1981, *Ap. J.*, **243**, 97.
Kellermann, K. I., and Pauliny-Toth, I. I. K. 1981, *Ann. Rev. Astr. Ap.*, **19**, 373.
Komesaroff, M. M., Roberts, J. A., Milne, D. K., Rayner, P. T., and Cooke, D. J. 1984, *M.N.R.A.S.*, **208**, 409.
Laing, R. A. 1980, *M.N.R.A.S.*, **193**, 439.

Ledden, J. E., and Aller, H. D. 1978, in *Pittsburgh Conference on BL Lac Objects*, ed. A. M. Wolfe (Pittsburgh: University of Pittsburgh Press), p. 60.
Moore, R. L., *et al.* 1982, *Ap. J.*, **260**, 415.
O'Dea, C. P., Balonek, T. J., Dent, W. A., and Kapitzky, J. E. 1982, in *Low Frequency Variability of Extragalactic Radio Sources*, ed. W. D. Cotton and S. R. Spangler (Green Bank, W. Va.: NRAO), p. 115.
Owen, F. N., Spangler, S. R., and Cotton, W. D. 1980, *Ap. J.*, **85**, 351.
Pauliny-Toth, I. I. K., Preuss, E., Witzel, A., and Graham, D. 1981, *A.J.*, **86**, 371.
Perley, R. A. 1982, *A.J.*, **87**, 859.
Phillips, R. B., and Mutel, R. L. 1982, *Ap. J.* (*Letters*), **257**, L19.
Preuss, E. 1982 in *Astrophysical Jets*, ed. A. Ferrari and A. Pacholczyk (Dordrecht: Reidel), p. 1.
Rayleigh, L. 1980, *Phil. Mag.*, **10**, 73.
Readhead, A. C. S., Hough, D. H., Ewing, M. S., Walker, R. C., and Romney, J. D. 1983, *Ap. J.*, **265**, 107.
Rudnick, L., and Jones, T. W. 1982, *Ap. J.*, **255**, 39.
———. 1983, *A.J.*, **88**, 518.
———. 1985, in preparation.
Rudnick, L., Jones, T. W., Edgar, B. K., and Pedelty, J. A. 1984, *A.J.*, **89**, 316.
Rudnick, L., Owen, F. N., Jones, T. W., Puschell, J. J., and Stein, W. A. 1978, *Ap. J.* (*Letters*), **225**, L15.
Rudnick, L., *et al.* 1985, *Ap. J. Suppl.*, **57**, in press.
Scheuer, P. A. G., and Readhead, A. C. S. 1979, *Nature*, **277**, 182.
Unwin, S. C., Mutel, R. L., Phillips, R. B., and Linfield, R. P. 1982, *Ap. J.*, **256**, 83.
Walker, R. C., Seielstad, G. A., Simon, R. S., Unwin, S. C., Cohen, M. H., Pearson, T. J., and Linfield, R. P. 1982, *Ap. J.*, **257**, 56.
Wardle, J. F. C. 1984, in *Proc. Green Bank Workshop: Physics of Energy Transport in Extragalactic Radio Sources, August 1984*, ed. A. Bridle and J. Eilek (Green Bank, W. Va.: NRAO), in press.
Weiler, K. W., and Johnston, K. J. 1980, *M.N.R.A.S.*, **190**, 269.

H. D. ALLER and M. F. ALLER: 953 Physics-Astronomy Bldg., University of Michigan, Ann Arbor, MI 48109

R. L. FIEDLER: Department of Physics and Astronomy, University of Iowa, Iowa City, IA 52242

P. E. HODGE: Space Telescope Science Institute, Homewood Campus, Baltimore, MD 21218

T. W. JONES and L. RUDNICK: Department of Astronomy, University of Minnesota, 116 Church Street, S.E., Minneapolis, MN 55455